BRAIN
ORIGINAL ARTICLE

Mitochondrial damage is associated with an early immune response in inclusion body myositis

Felix Kleefeld,[1,2,†] Emily Cross,[3,†] Daniel Lagos,[3] Sara Walli,[4] Benedikt Schoser,[5] Andreas Hentschel,[6] Tobias Ruck,[4] Christopher Nelke,[4] Katrin Hahn,[1] Denisa Hathazi,[3] Andrew L. Mammen,[7,8] Maria Casal-Dominguez,[7,8] Marta Gut,[9,10] Ivo Glynne Gut,[9,10] Simon Heath,[9,10] Anne Schänzer,[11,12] Hans-Hilmar Goebel,[13] Iago Pinal-Fernandez,[7,8,‡] Andreas Roos,[6,14,15,‡] Corinna Preuße,[13,‡] Werner Stenzel[13,†] and Rita Horvath[3,†]

[†,‡]These authors contributed equally to this work.

Polymyositis with mitochondrial pathology (PM-Mito) was first identified in 1997 as a subtype of idiopathic inflammatory myopathy. Recent findings demonstrated significant molecular similarities between PM-Mito and inclusion body myositis (IBM), suggesting a trajectory from early to late IBM and prompting the inclusion of PM-Mito as an IBM precursor (early IBM) within the IBM spectrum. Both PM-Mito and IBM show mitochondrial abnormalities, suggesting that mitochondrial disturbance is a crucial element of IBM pathogenesis.

The primary objective of this cross-sectional study was to characterize the mitochondrial phenotype in PM-Mito at histological, ultrastructural and molecular levels and to study the interplay between mitochondrial dysfunction and inflammation. Skeletal muscle biopsies of 27 patients with PM-Mito and 27 with typical IBM were included for morphological and ultrastructural analysis. Mitochondrial DNA (mtDNA) copy number and deletions were assessed by quantitative PCR and long-range PCR, respectively. In addition, full-length single-molecule sequencing of the mtDNA enabled precise mapping of deletions. Protein and RNA levels were studied using unbiased proteomic profiling, immunoblotting and bulk RNA sequencing. Cell-free mtDNA was measured in the serum of IBM patients.

We found widespread mitochondrial abnormalities in both PM-Mito and IBM, illustrated by elevated numbers of cytochrome c oxidase (COX)-negative and succinate dehydrogenase (SDH)-positive fibres and prominent ultrastructural abnormalities, with disorganized and concentric cristae within enlarged and dysmorphic mitochondria. mtDNA copy numbers were significantly reduced, and multiple large-scale mtDNA deletions were already evident in PM-Mito compared with healthy age-matched controls, similar to the IBM group. The canonical cyclic GMP–AMP synthase/stimulator of interferon genes inflammatory pathway was activated in PM-Mito and IBM, and we detected elevated levels of circulating cell-free mtDNA indicative of mtDNA leakage. In PM-Mito and IBM, these findings were accompanied by dysregulation of proteins and transcripts linked to the mitochondrial membranes.

In summary, we identified that mitochondrial dysfunction with multiple mtDNA deletions and depletion, disturbed mitochondrial ultrastructure and defects of the inner mitochondrial membrane are features of PM-Mito and IBM, underlining the concept of an IBM-spectrum disease. Notably, mitochondrial abnormalities precede tissue remodelling and infiltration by specific T-cell subpopulations (e.g. KLRG1^{+}) characteristic of late IBM. The activation of inflammatory, DNA-sensing pathways might be related to mtDNA release, which would indicate a significant role of mitochondria-associated inflammation in the pathogenesis of IBM-spectrum disease. This study highlights the crucial role of early mitochondrial abnormalities in the pathomechanism of IBM, which might lead to new approaches to therapy.

Received August 02, 2024. Revised February 27, 2025. Accepted March 18, 2025. Advance access publication April 7, 2025

1 Department of Neurology, Berlin Institute of Health (BIH), Charité-Universitätsmedizin Berlin, Corporate member of Freie Universität Berlin, Humboldt, Universität zu Berlin, 10117 Berlin, Germany
2 Department of Neurology, Heimer Institute for Muscle Research, University Hospital Bergmannsheil, Ruhr-University Bochum, 44789 Bochum, Germany
3 Department of Clinical Neurosciences, University of Cambridge, Cambridge CB2 0QQ, UK
4 Department of Neurology, Medical Faculty, Heinrich Heine University Düsseldorf, 40225 Düsseldorf, Germany
5 Department of Neurology, Friedrich-Baur-Institute, Ludwig-Maximilians-University, 80336 Munich, Germany
6 Leibniz-Institut für Analytische Wissenschaften—ISAS e.V., 44139 Dortmund, Germany
7 Muscle Disease Unit, National Institute of Arthritis and Musculoskeletal and Skin Diseases, National Institutes of Health, Bethesda, MD 20892, USA
8 Department of Neurology, Johns Hopkins University School of Medicine, Baltimore, MD 21205, USA
9 Centro Nacional de Análisis Genómico (CNAG), 08028 Barcelona, Spain
10 Universitat de Barcelona (UB), Barcelona Institute of Science and Technology (BIST), Universitat Pompeu Fabra (UPF), 08002 Barcelona, Spain
11 Institute of Neuropathology, Justus Liebig University, 35392 Giessen, Germany
12 Translational Neuroscience Network Giessen (TNGG), Justus Liebig University Giessen, 35392 Giessen, Germany
13 Department of Neuropathology, Berlin Institute of Health (BIH), Charité-Universitätsmedizin Berlin, Corporate member of Freie Universität Berlin, Humboldt-Universität zu Berlin, 10117 Berlin, Germany
14 Department of Pediatric Neurology, Centre for Neuromuscular Disorders, Centre for Translational Neuro- and Behavioral Sciences, University Duisburg-Essen, 45147 Essen, Germany
15 Brain and Mind Research Institute, Children's Hospital of Eastern Ontario Research Institute, University of Ottawa, Ottawa, ON K1H 8L1, Canada

Correspondence to: Rita Horvath
Department of Clinical Neurosciences, University of Cambridge
Forvie Site, Robinson Way, Cambridge CB2 0PY, UK
E-mail: rh732@medschl.cam.ac.uk

Correspondence may also be addressed to: Werner Stenzel
Department of Neuropathology, Berlin Institute of Health (BIH), Charité-Universitätsmedizin Berlin
Corporate member of Freie Universität Berlin, Humboldt-Universität zu Berlin
Charitéplatz 1, 10 117 Berlin, Germany
E-mail: werner.stenzel@charite.de

Keywords: polymyositis with mitochondrial pathology; inclusion body myositis-spectrum disease; mitochondria

Introduction

Polymyositis with mitochondrial pathology (PM-Mito), first identified in 1997 as a subtype of idiopathic inflammatory myopathy, is characterized by significant mitochondrial abnormalities and inflammation.[1] Recently, we described a considerable histological and molecular overlap between PM-Mito and inclusion body myositis (IBM).[2] We showed that >90% of patients diagnosed with PM-Mito developed IBM in their later course, which was confirmed by follow-up biopsies several years apart, and we proposed inclusion of PM-Mito as an early form of IBM within the spectrum of IBM (IBM-spectrum disease, IBM-SD).[2] Although specific inflammatory features and characteristic tissue damage of skeletal muscle, including protein aggregates and rimmed vacuoles, are less pronounced in PM-Mito compared with typical IBM, we observed a similar quantity and quality of mitochondrial abnormalities defined by light microscopy [cytochrome c oxidase (COX)-negative and succinate dehydrogenase (SDH)-positive fibres], pointing towards mitochondrial abnormalities and likely dysfunction being an early feature of IBM. Indeed, multiple mitochondrial DNA (mtDNA) deletions, typically seen in IBM, have also been reported in smaller cohorts of PM-Mito patients.[3] However, mitochondrial abnormalities in PM-Mito have not been studied in depth. Mitochondrial morphological abnormalities with multiple mtDNA deletions and depletion were shown to be a characteristic feature of IBM.[4,5] However, the mechanisms linking these mitochondrial abnormalities and inflammation to the pathogenesis of IBM remained puzzling.

Recently, abnormal mitochondria have been reported to contribute to interferon-mediated inflammation in dermatomyositis by activating the canonical cyclic GMP–AMP synthase/stimulator of interferon genes (cGAS/STING) pathway.[6] CGAS/STING activation has also been identified in other idiopathic inflammatory myopathies, including immune-mediated necrotizing myopathy,[7] and in a range of autoinflammatory syndromes, such as hereditary interferonopathies.[8] Notably, the role of the cGAS/STING pathway in IBM remains unknown to date.

In IBM, a link has been suggested between degenerative features (e.g. TDP-43 deposition) and mitochondrial pathology.[9] These findings have led to the assumption that IBM might be a primary degenerative disease of skeletal muscle.[10] Moreover, this hypothesis has been supported by the failure of previous immunosuppressive treatment strategies. However, IBM also shows distinct features of a complex immune-mediated disorder, possibly involving cytosolic 5′-nucleotidase 1A (cN1A) antibodies, $CD8^+$ lymphocytes,

macrophages and cytokines, such as interferons (IFN).[11-13] Yet, immunization with cN1A antibodies could reproduce only inflammatory features but no mitochondrial abnormalities in mice.[14] Despite extensive research, whether mitochondrial dysfunction should be viewed as a downstream consequence of persistent inflammation or mitochondria might be at the core of disease pathophysiology remains unsolved.

In the present study, we hypothesized that mitochondrial dysfunction is an early feature of IBM and might be linked mechanistically to the development of autoimmunity and inflammation. Studying a well-characterized, unique cohort of PM-Mito muscle biopsy specimens, our primary research focused on providing an in-depth characterization of the mitochondrial phenotype observed in PM-Mito at the histological, ultrastructural and molecular levels. In addition, we investigated the interplay between early mitochondrial damage and activation of canonical inflammatory pathways. We identified that mitochondrial dysfunction, including multiple mtDNA deletions and mtDNA depletion, along with disturbed mitochondrial ultrastructure and membrane defects, is an early feature of IBM. Activation of inflammatory pathways related to mtDNA release highlights the significant role of mitochondria-associated inflammation in IBM pathogenesis, where mitochondrial abnormalities precede tissue remodelling and T-cell infiltration.

Materials and methods

For this study, experiments were conducted in Berlin, Germany (Charité-Universitätsmedizin Berlin, Department of Neuropathology; histology and electron microscopy), Cambridge, UK [University of Cambridge, Department of Clinical Neurosciences; immunoblotting, long-range and quantitative PCR (qPCR)], Barcelona, Spain [Centro Nacional de Análisis Genómico (CNAG); nanopore sequencing of mtDNA], Dortmund, Germany (Leibniz-Institut für Analytische Wissenschaften-ISAS e.V.; unbiased proteomic profiling) and Bethesda, MD, USA (the National Institutes of Health; bulk RNA sequencing). Approval for the study was obtained from the institutional ethics review board of Charité-Universitätsmedizin Berlin (EA2/107/14 and EA1/019/22), and a Material Transfer Agreement (MTA) was established between the participating institutions. The study adhered to the principles outlined in the 1964 Declaration of Helsinki, and patient and control data were anonymized following the guidelines of the local institutional ethics review board.

Patients, samples and clinical assessment

This study included skeletal muscle biopsy specimens showing signs of polymyositis with mitochondrial pathology (referred to as 'PM-Mito') and clinically and pathologically confirmed IBM according to the 2011 European Neuromuscular Centre (ENMC) criteria.[15] The definition of PM-Mito was based on established histopathological criteria, including endomysial inflammation, invasion of non-necrotic muscle fibres, and >3% of muscle fibres with deficient COX activity (visualized by combined COX–SDH enzyme histochemical preparations).[1] Using these criteria, PM-Mito is defined as an inflammatory myopathy ('polymyositis') characterized by pronounced mitochondrial dysfunction and the absence of vacuoles, the latter serving as the key pathological feature distinguishing it from IBM. Clinical and serological (auto-antibodies) features were not considered when classifying PM-Mito patients, to ensure comparability with previous studies on PM-Mito. All available biopsies with signs of PM-Mito were included from the cohorts in Berlin and Giessen, Germany. To minimize selection bias, IBM biopsies were selected randomly from available samples in Berlin without preselection based on comorbidities, sex or antibody status. Control biopsy specimens from individuals with normal creatine kinase levels, negative myositis line blots (Myositis profile 4 EUROLINE immunoblot; EUROIMMUN AG, Lübeck, Germany) and unremarkable skeletal muscle morphology were also included. None of the controls had a family history of neuromuscular disease. All biopsies were obtained for diagnostic purposes at Charité-Universitätsmedizin Berlin, Germany, and Justus Liebig University Giessen, Germany, and analysed by myopathologists (H.-H.G., W.S., F.K. and A.S.). All patients' medical data, including a complete neurological examination at the time of biopsy, were collected. In addition, laboratory data (creatine kinase; myositis line blot) were collected.

Skeletal muscle biopsies

We examined skeletal muscle biopsy specimens from PM-Mito ($n = 27$) and IBM ($n = 27$) patients, all sourced from quadriceps femoris muscles. The specimens were snap-frozen and cryopreserved at −80°C before histological and immunohistochemical analysis or fixed and embedded directly after the biopsy for transmission electron microscopy.

Histological and immunohistochemical analysis

Samples were processed following standardized protocols at the Department of Neuropathology, Charité-Universitätsmedizin, Berlin. Routine staining, immunohistochemical and double immunofluorescence reactions were carried out as described previously.[2,16,17] In short, the 7-µm-thick cryostat sections were stained with haematoxylin and eosin, modified Gömöri trichrome, for non-specific esterase, alkaline phosphatase, etc., as described in a consensus statement,[18] and with a comprehensive panel of antibodies for immunohistochemistry and double immunofluorescence as described previously.[16,17] Double immunofluorescence was performed after blocking with the appropriate serum [1:10 in phosphate buffered saline (PBS)], dependent upon the source of the secondary antibody, and incubated with primary antibodies for 1 h at room temperature. The secondary antibody was added for 1 h. This was repeated with the second primary antibody and appropriate secondary antibodies. The sections were mounted aqueously and stored at 4°C. The following antibodies were used for immunohistochemistry: C5b-9 (Dako, aE11, 1:200), CD8 (Dako, C8/144B, 1:100), CD45 (Dako, 2B11, 1:400), CD56 (Serotec/MCA591 ERIC-1, 1:400), CD57 (Zymed, SPM129, 1:50), CD68 (Dako, EBM11, 1:100), major histocompatibility complex (MHC) class I (Dako, w6/32, 1:1000), MHC class II (Dako, CR3/43, 1:100), SQSTM1/p62 (Abcam, polyclonal, 1:100) and KLRG-1 (Proteintek, 10974-1-AP, 1:50). Appropriate positive and negative controls (tissue reactions) were used where necessary. Additionally, histologically normal muscles (e.g. for MHC class I or II positivity of capillaries) were used as negative controls for immunohistochemical reactions.

The above-mentioned comprehensive antibody panel was also used to ensure negative staining results by studying so-called 'irrelevant antibodies' for validation. 'Irrelevant antibodies' are used to ensure the specificity of staining and to maintain quality control standards. These are antibodies directed against antigens not present in the tissue under investigation, serving as negative controls to validate staining results. For quantification of mitochondrial morphological alterations (i.e. COX negativity) and immune cells ($CD8^+$ T cells, $CD68^+$ macrophages and $CD45^+$ leucocytes), muscle fibres and immune cells were counted in 10 high power fields (based on the microscope used and the respective oculars (Olympus WH10x-H/22), ~0.16 mm^2).

Transmission electron microscopy

For transmission electron microscopy, muscle biopsy specimens were fixed and embedded according to standard protocols and as described previously.[19] In brief, muscle specimens were fixed in 2.5% glutaraldehyde diluted in 0.1 M sodium cacodylate buffer for a minimum of 24 h at 4°C, osmicated in 1% osmium tetroxide in 0.05 M sodium cacodylate buffer, dehydrated using a graded acetone series including combined *en bloc* staining with 1% uranyl acetate and 0.1% phosphotungstic acid in 70% acetone, infiltrated in RenLam resin, then polymerized for 48–72 h at 60°C. Semithin sections (500 nm) were stained with Richardson solution (methylene blue) for microanatomical examination. Ultrathin sections (60–70 nm) were stained with uranyl acetate and lead citrate. Next, ultrastructural analysis was performed using TEM 902 and TEM 906 (Zeiss).

Unbiased proteomic studies

Muscle biopsy specimens were prepared for proteomic analysis following established protocols and as described previously.[20] The analysis included 14 samples from PM-Mito patients and 10 from IBM patients. The PM-Mito cohort included 11 female and 3 male patients with a mean age of 64.9 years (±12.4 years). The IBM cohort included four female and six male patients with a mean age of 70.7 years (±5.8 years). Five age-matched adult male and two female patients with normal family histories, histological studies and laboratory work-ups served as controls. These individuals were biopsied diagnostically for muscle pain but showed no pathological changes upon microscopic examination. Using a bottom-up unbiased proteomic approach[21] with label-free peptide quantification based on our previously published data-independent-acquisition (DIA) workflow,[20] we relatively quantified proteins based on detecting a minimum of more than two unique peptides in the PM-Mito and control groups. The mass spectrometry proteomics data have been deposited into the ProteomeXchange Consortium via the PRIDE partner repository,[22] with the dataset identifier PXD053742.

For the statistical analysis of proteomic data, each dataset was converted into a standardized format, with sample identifiers as row names and protein measurements as columns. To address missing values in the proteomics datasets, an imputation approach was implemented. Missing values were replaced by random draws from a truncated normal distribution with parameters adjusted relative to the distribution of observed values: the mean was shifted by 1.8 times the SD, and the SD was scaled by 30%. Imputed values were logged to match the distribution of observed data. A binary column tracked imputed data points for transparency. Columns with zero variance were identified and removed from the datasets to ensure meaningful downstream analyses. This step eliminated potential artefacts from invariant features. Principal component analysis (PCA) was performed on the datasets to visualize sample groupings and explore variance explained by the primary components. Data were scaled and centred prior to principal component analysis. Principal component analysis plots were generated to display the first two principal components, with samples colour-coded by their corresponding groups in the annotation table. Ellipses representing 95% confidence intervals for each group were overlaid on the plots. To identify differentially expressed proteins, Welch's *t*-tests were conducted between groups for each protein. Log2 fold changes were calculated to measure the relative expression levels. Multiple testing correction was performed using the fdrtool package to compute *q*-values, ensuring control of the false discovery rate. A volcano plot was generated to visualize the results of the differential expression analysis. Proteins were plotted based on their log2 fold change and *q*-value. Gene set enrichment analysis (GSEA) was performed using GeneTrail v.3.2 using standard settings for GSEA and the Kolmogorov–Smirnov test.

Immunoblotting

Muscle biopsy samples were lysed in 100 µl of lysis buffer: 50 mM Tris–HCl (Applichem Biochemica A3452), pH 7.8, 150 mM NaCl (Merck), 1% sodium dodecyl sulphate (Carl Roth) and supplemented with proteases/phosphatases inhibitors (Roche), using a manual glass grinder followed by sonication. Samples were centrifuged at 4°C for 5 min at 5000*g*. The protein concentration of the supernatant was determined with the Pierce™ Rapid Gold BCA Protein Assay Kit (Thermo Fisher) according to the manufacturer's protocol.

For immunoblotting, 10 µg of total protein extract was used for each sample analysed. The samples were loaded on a gradient polyacrylamide gel (NuPage 4%–12% Bis-Tris Protein gel, Thermo Fisher) and separated for 60 min at 150 V. Proteins were then transferred to a polyvinylidene fluoride membrane (Invitrogen transfer stacks) using the iBlot2 dry transfer system (Thermo Fisher) according to the manufacturer's protocol. Membranes were blocked with 5% milk powder diluted in PBS (Gibco) or Tris-buffered saline (Santa Cruz) with 0.1% Tween-20 (Sigma-Aldrich) for 2 h and four washing steps using PBS with Tween 20 (PBS-T). Membranes were next incubated with primary antibodies (Total OXPHOS Human WB Antibody Cocktail, Abcam, ab110411; dilution 1:800; TOM20: Recombinant Anti-TOM20 antibody, ab186735, dilution 1:2000; GAPDH: Anti-GAPDH antibody, ab8245, dilution 1:2000, ATP5a: Abcam, ab14748, dilution 1:2000; CHCHD3: Proteintech, 25625-1-AP, dilution 1:5000; ATAD3a: Abcam, ab112572, dilution: 1:1000; SAM50: Proteintech, 28679-1-AP, dilution: 1:1000; TIM23: Abcam, ab230253, dilution 1:1000; VDAC1: Abcam, ab14734, dilution: 1:1000; STING: Cell Signaling Technologies, 13647, dilution 1:1000; pSTING: Cell Signaling Technologies, 50907, dilution 1:1000; CASP-1: Proteintech, 22915-1-AP, dilution 1:5000; and ACTB: Proteintech, dilution 1:5000) at 4°C overnight, then washed three times in 1× PBS-T. Horseradish peroxidase-conjugated secondary goat anti-mouse antibody (Thermo Fisher) and goat anti-rabbit (Thermo Fisher) antibodies were diluted at 1:5000 and added to the membranes for 2 h. Imaging was performed after washing polyvinylidene fluoride membranes three times in PBS-T for 10 min using enhanced chemiluminescence and a horseradish peroxidase substrate (Super-Signal West Femto, Pierce). Signals were detected using an Amersham Imager 680 machine (GE Life Sciences). GAPDH was used as a loading control, and mitochondrial content was normalized to the mitochondrial protein TOM20. Three control muscle biopsy specimens were used, from patients who were biopsied diagnostically for muscle pain but showed no pathological changes upon microscopic examination.

Quantification of mtDNA copy number

Following a previously published protocol, the relative mtDNA copy number per cell was quantified by a multiplex Taqman qPCR assay (Bio-Rad).[23] *B2M* transcript levels were used as nuclear-encoded reference gene, and *MT-ND1* was used as a mitochondrial-encoded gene. The primers used for the qPCR reaction were as follows: *B2M* forward 5′-CACTGAAAAAGATGAGTATGCC-3′ and reverse 5′-AACATTCCCTGACAATCCC-3′; and *MT-ND1* forward 5′-ACGCCATAAAACTCTTCACCAAAG-3′ and reverse 5′-GGGTTCAT AGTAGAAGAGCGATGG-3′. All samples were run in triplicate, and

replicates with a difference of >0.5C_t were removed. The relative amount of mtDNA was calculated as the difference in cycle threshold (C_t) value of *B2M* and *MT-ND1*, where ΔC_t equals the sample C_t of the mitochondrial gene (*MT-ND1*) subtracted from the sample C_t of the nuclear reference gene (*B2M*). Six healthy and age-matched controls (four females and two males, >50 years of age) were included for this analysis.

Long-range PCR for mitochondrial DNA deletions

The presence of mtDNA deletions in the major arc (10 kb) of the mitochondrial genome was assessed by long-range PCR. Custom-made primers were used (forward 5′-CCCTCTCTCCTACTCCTG-3′ and reverse 5′-CAGGTGGTCAAGTATTTATGG-3′). PCR amplification was performed on a T100 Thermal Cycler (Bio-Rad) using 1 µl of DNA and PrimeSTAR GXL DNA Polymerase (Takara Bio Europe) according to the manufacturer's recommendations. PCR products were electrophoresed on a 0.7% agarose gel for 65 min. Three healthy and age-matched controls (two male and one female) were included in the analysis.

Multiplexed full-length single-molecule sequencing of the mitochondrial genome by Cas9-mtDNA Oxford nanopore sequencing

We applied a method to target, multiplex and sequence at high coverage full-length human mitochondrial genomes as native single molecules, using the RNA-guided DNA endonuclease Cas9 (for detailed methods, see Keraite *et al.*[24]). Combining Cas9-induced breaks that define the mtDNA beginning and end of the sequencing reads as barcodes, we achieved high demultiplexing specificity and delineation of the full-length mtDNA, regardless of the structural variant pattern. The long-read sequencing data were analysed using a pipeline with custom-developed software, Baldur, which efficiently detects single nucleotide heteroplasmy to <1%, physically determines the phase and can accurately disentangle complex deletions.

Bulk RNA sequencing

Bulk RNA sequencing was performed on frozen muscle biopsy specimens as previously described.[25] In short, RNA was extracted from fresh-frozen biopsies using TRIzol (Invitrogen) and quantified using NanoDrop. Libraries for bulk RNA sequencing were prepared using NEBNext Poly(A) mRNA Magnetic Isolation Module and Ultra II Directional RNA Library Prep Kit for Illumina (New England BioLabs, Cat. Nos. E7490 and E7760). The input RNA and the resulting libraries were analysed with Agilent 4200 Tapestation for quality assessment. Transcript levels are reported as log2[trimmed mean of M-values (TMM) + 1]. Histologically normal muscle biopsies were included as controls. These samples were obtained from the Johns Hopkins Neuromuscular Pathology Laboratory (n = 12), the skeletal muscle biobank of the University of Kentucky (n = 8) and the National Institutes of Health (n = 13). The normal muscle biopsies from the Johns Hopkins Neuromuscular Pathology Laboratory were obtained for clinical purposes but did not show any histological abnormality; the rest of the normal biopsies were obtained from healthy volunteers. Pathway analysis was done using GSEA with clusterProfiler/4.12.6 and enrichplot/1.24.4 for the Reactome and the Hallmark datasets.[26]

Quantification of cell-free mtDNA from serum

Serum samples were available from nine IBM patients and nine healthy age-matched controls and cryopreserved at −80°C. For DNA extraction, 100 µl of serum was centrifuged at 2000*g* for 5 min to remove debris and processed using the DNeasy Blood and Tissue Kit (Qiagen), with the ethanol precipitation step performed overnight at −20°C. Samples were concentrated to half the volume using DNA110 SpeedVac. Equal volumes of DNA were loaded for mtDNA copy number qPCR as described above, with the addition of the *MT-ND4* marker. The primers used for *MT-ND4* were as follows: forward 5′-ACCTTGGCTATCATCACCCGAT-3′ and reverse 5′-AGTGCGATGAGTAGGGGAAGG-3′. Relative *MT-ND1* and *MT-ND4* copy number were calculated by multiplying C_t values from the calculation 2×2^{-Ct} and normalizing values to the average of the controls. Two outliers from the control group were removed after subsequent statistical testing.

Quantification and statistical analysis

Categorical variables are reported as numbers and percentages and were compared using Fisher's exact test. Quantitative variables are reported as the mean (±SD) and compared using Mann–Whitney or Kruskal–Wallis with Dunn's multiple comparison tests. Spearman rank-order correlations were used to calculate the association's quantitative variables. A P-value of <0.05 was considered significant. Outliers were identified and removed using the ROUT method at Q = 1%. GraphPad Prism v.9.2.0 (GraphPad Software, Inc., La Jolla, CA, USA) was used for analysis.

Results

Clinical and demographic data of the patient cohorts

Our study included skeletal muscle biopsy specimens from 27 patients with PM-Mito (22 female and 5 male) and 27 patients with typical IBM (13 female and 14 male), meeting the ENMC criteria for clinicopathologically defined IBM.[15] We previously reported the clinical features of these cohorts in detail.[2] Significantly, the two patient groups did not differ in age at biopsy (PM-Mito 66 ± 12 years, IBM 69 ± 9.2 years, P = 0.25). All patients with IBM presented with the pathognomonic clinical pattern, whereas PM-Mito patients showed a spectrum of clinical symptoms. The most common clinical presentations at the time of muscle biopsy for PM-Mito patients were proximal muscle weakness (bilateral quadriceps femoris muscle weakness) and other incomplete IBM-like patterns not meeting 2011 ENMC criteria (e.g. isolated knee extensor weakness, long finger and wrist flexor weakness). Creatine kinase levels were moderately elevated [≤10 × the upper limit of normal (≥174 U/l)] in both groups, again without statistically significant differences (data not shown). In the PM-Mito group, only one patient (PM 23) tested positive for anti-cN1A antibodies, whereas in the IBM subgroup, 6/27 patients (IBM 1, 5, 8, 9, 10 and 13) tested positive for anti-cN1A antibodies. Twelve PM-Mito and nine IBM patients were ANA-positive with low titres (≤1:320). Two PM-Mito patients (PM 6 and 21) had equivocal TIF1-gamma antibody results, but retesting was negative in both cases. None of the patients in this cohort exhibited myositis-associated skin manifestations.

As previously reported,[27] all late IBM and 16/27 PM-Mito patients have received immunosuppressive/immunomodulatory treatment before and/or after muscle biopsy, which has not led to sustained clinical improvement in any of the patients. Immunotherapy consisted of intravenous immunoglobulin treatment in all IBM patients (according to the German Myositis Treatment guidelines). PM-Mito patients were treated with methotrexate (10/27), azathioprine (6/27) and corticosteroids (14/16). However, none of the IBM and

Table 1 Demographic and clinical characteristics of PM-Mito and IBM patients

Patient	Age at biopsy (years)	Sex	Clinical pattern	Patient	Age at biopsy (years)	Sex	Clinical pattern
PM 1	64	F	IBM pattern	IBM 1	75	F	IBM pattern
PM 2	51	F	Prox. paraparesis	IBM 2	72	F	IBM pattern
PM 3	68	F	Prox. paraparesis	IBM 3	66	M	IBM pattern
PM 4	57	F	Prox. paraparesis	IBM 4	77	M	IBM pattern
PM 5	76	F	Prox. paraparesis	IBM 5	64	F	IBM pattern
PM 6	52	M	Prox. paraparesis	IBM 6	69	M	IBM pattern
PM 7	83	F	Prox. paraparesis	IBM 7	62	M	IBM pattern
PM 8	56	F	Asymptomatic	IBM 8	75	M	IBM pattern
PM 9	78	F	Prox. tetraparesis	IBM 9	61	F	IBM pattern
PM 10	48	F	Prox. tetraparesis	IBM 10	63	F	IBM pattern
PM 11	81	F	Prox. paresis upper limbs	IBM 11	73	F	IBM pattern
PM 12	77	F	Prox. paraparesis	IBM 12	75	M	IBM pattern
PM 13	73	F	Prox. tetraparesis	IBM 13	86	M	IBM pattern
PM 14	79	F	Prox. paraparesis	IBM 14	45	F	IBM pattern
PM 15	67	M	Prox. tetraparesis	IBM 15	83	F	IBM pattern
PM 16	52	F	Asymptomatic	IBM 16	58	M	IBM pattern
PM 17	60	F	Prox. paresis upper limbs	IBM 17	55	F	IBM pattern
PM 18	51	F	Myalgia	IBM 18	58	M	IBM pattern
PM 19	55	M	Myalgia	IBM 19	66	F	IBM pattern
PM 20	68	M	Myalgia	IBM 20	67	F	IBM pattern
PM 21	77	M	Prox. tetraparesis	IBM 21	72	M	IBM pattern
PM 22	69	M	IBM pattern	IBM 22	78	F	IBM pattern
PM 23	60	F	IBM pattern	IBM 23	72	F	IBM pattern
PM 24	70	M	IBM pattern	IBM 24	69	F	IBM pattern
PM 25	52	F	Prox. tetraparesis	IBM 25	68	M	IBM pattern
PM 26	84	F	IBM pattern	IBM 26	60	M	IBM pattern
PM 27	79	F	IBM pattern	IBM 27	81	M	IBM pattern

F = female; IBM = inclusion body myositis; M = male; prox. = proximal; PM-Mito = polymyositis with mitochondrial pathology.

only four patients in the PM-Mito subgroup received immunosuppressive/immunomodulatory treatment with low-dose (7.5–20 mg daily) oral prednisolone at the time of biopsy (see Table 1; PM 2, 6, 10 and 13). No other patients received immunosuppressants within 3 months before the biopsy.

Functional, structural and molecular alterations of mitochondria

COX-negative/SDH-positive muscle fibres were present in both PM-Mito and IBM muscle

Twenty-seven muscle biopsy specimens derived from PM-Mito patients were available for comprehensive histological analysis, and 27 randomly selected specimens showing classic IBM features were studied. All muscle biopsy samples showed a combination of mild to moderate fibre-size variation, with endomysial lymphomonocytic infiltrates, mildly increased numbers of internalized myonuclei and intense sarcolemmal staining by MHC class I (Fig. 1). Focal MHC class II positivity was observed, particularly in areas with $CD8^+$ T-cell infiltrates. As published previously, vacuoles and $p62^+$ intracellular aggregates were absent in all PM-Mito cases,[2] because these would classify these cases as IBM according to the ENMC criteria.

PM-Mito skeletal muscle biopsy specimens revealed small clusters of infiltrates (Fig. 1, top row) of T cells within the endomysium, often encircling individual myofibres or small groups of myofibres with interspersed macrophages. All PM-Mito muscle biopsy specimens showed an increased amount of COX-negative (SDH-positive) muscle fibres for the patients' age according to established criteria (i.e. >3% of muscle fibres).[28] Quantifying COX-negative muscle fibres revealed no statistical difference in the percentage and total amount of COX-negative fibres per 10 high power fields between PM-Mito cases (4.2% ± 2.1%) and typical IBM cases (4.8% ± 2.4%; $P = 0.33$; see Supplementary Table 1). Mitochondrial abnormalities were evident throughout all stages of the disease, including very mild cases with few inflammatory infiltrates. Three representative PM-Mito cases showing only mild myopathic alterations, without evident fatty–fibrotic tissue remodelling and with few infiltrates but pronounced mitochondrial abnormalities in COX/SDH stains, are illustrated in Fig. 1.

Distinct ultrastructural mitochondrial abnormalities in PM-Mito and IBM

Transmission electron microscopy was performed on 10 randomly selected PM-Mito cases and 10 IBM cases. Overall, in transmission electron microscope studies, all muscle biopsy specimens showed mitochondrial abnormalities with quantitative rather than qualitative differences between the individual patients. Non-specific signs, such as swollen, elongated and dysmorphic mitochondria and subsarcolemmal accumulation, were present in all PM-Mito and IBM cases. We also observed discontinuity of the mitochondrial membranes, accompanied by leakage of mitochondrial content into the sarcoplasm, which was observed in both patient groups in 70% of the electron microscope images (Fig. 2A). Other features included paracrystalline inclusions (Fig. 2B) type 1 and 2, concentric cristae (Fig. 2C) and giant mitochondria with densely packed cristae membranes (GM[29]; Fig. 2D). We quantified these distinct ultrastructural abnormalities in PM-Mito and IBM cases at 12 000- to 20 000-fold magnification. Paracrystalline inclusions were detected in 8.7% of PM-Mito and in 12.6% of IBM mitochondria. Concentric cristae were found in 10.8% and 11.8%, and GM in 0.6% and 12.6% of mitochondria, respectively. Mitophagy was occasionally seen but was not a prominent ultrastructural finding. None of the control

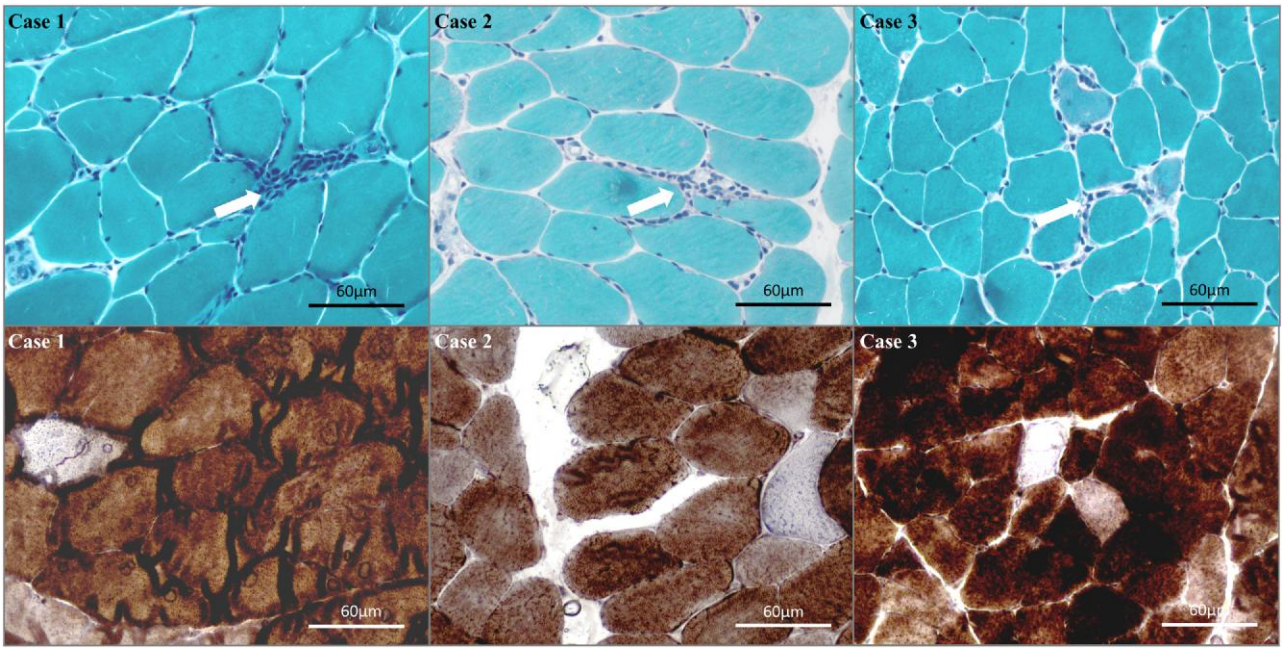

Figure 1 Inflammation and mitochondrial dysfunction in three cases of PM-Mito. Cases 1–3 illustrate muscle biopsy specimens with few inflammatory infiltrates (arrows) but pronounced mitochondrial abnormalities, evident as COX-deficient myofibres. *Top row*: Gömöri trichrome stain. *Bottom row*: COX-SDH histochemistry. COX = cytochrome c oxidase; PM-Mito = polymyositis with mitochondrial pathology; SDH = succinate dehydrogenase.

samples exhibited the above-mentioned mitochondrial changes. In summary, ultrastructural abnormalities of mitochondria were detected throughout all stages of the disease, including cases showing very mild signs of inflammation. However, giant mitochondria with densely packed cristae were more abundant in typical IBM cases.

Multiple mtDNA deletions and depletion are early signs of IBM-SD

PCR-based mtDNA copy number measurements were performed on 10 PM-Mito, 8 IBM and 13 control muscle biopsy specimens (Fig. 3A). The level of mtDNA showed a statistically significant reduction in PM-Mito patients (7.1 ± 0.91) and typical IBM patients (6.57 ± 0.88) compared with healthy, old-age control specimens (8.2 ± 0.61, Fig. 3A). Of note, there was no difference between the PM-Mito and IBM groups ($P = 0.33$); however, mtDNA copy numbers were significantly different in both PM-Mito ($P = 0.0077$) and IBM ($P = 0.0002$) compared with controls, indicating that the mtDNA defect is maintained throughout all stages of the disease.

To investigate further a possible link between mitochondrial dysfunction and deletions of the mtDNA, we performed a long-range PCR of the major arc, where most mtDNA deletions are known to be located.[30] Nine PM-Mito, five typical IBM and five control cases were studied using this technique. Given that mtDNA deletions are known to accumulate in ageing skeletal muscle, controls representing a similar age range (50–83 years) were included. We detected a similarly high number of multiple mtDNA deletions in PM-Mito and IBM (Fig. 3B), suggesting that mtDNA deletions arise early in the pathophysiology of the disease.

Multiplexed full-length single-molecule sequencing of the mitochondrial genome

We detected a large number of multiple mtDNA deletions of different sizes in both PM-Mito ($n = 8$) and IBM ($n = 9$) samples, much more than in age-matched controls ($n = 7$) (Fig. 3C). All samples showed deletions, with a range of sizes and heteroplasmy rates between ~1% and >50% (median ~11%). Deletions tend to cover regions from 8 to 12 kb, but deleted regions often span large regions from 3 to 16 kb. The number of single nucleotide mutations in the mtDNA was less prominent in the patient samples than mtDNA deletions.

The number of mtDNA deletions was significantly higher in IBM-SD (IBM and PM-Mito) patient samples than in controls, but not significantly different between PM-Mito and IBM patients ($P = 0.82$; Fig. 3C). The heteroplasmy rate was slightly higher in PM-Mito than in IBM, but did not reach statistical significance. These results confirm data obtained by long-range PCR analysis indicating that the mtDNA alterations are early signs of the pathology.

Unbiased proteomic profiling and bulk RNA sequencing

We performed unbiased proteomic profiling of 14 PM-Mito and 10 IBM muscle biopsy specimens. We detected 3787 proteins using this approach, of which 33 were statistically significantly downregulated and 20 were upregulated in PM-Mito patient samples versus controls. Principal component analysis showed segregation of non-disease controls (NDC), PM-Mito and IBM patients. PM-Mito patients clustered between NDC and IBM, reflecting the proteomic characteristics of skeletal muscle with mild to moderate pathological alterations (Fig. 4A). Interestingly, 11/33 downregulated proteins were linked to mitochondrial function, including complexes I and III of the respiratory chain, and 2 of the 10 most downregulated proteins were related to the inner mitochondrial membrane (SMDT1 and TIM21; Fig. 4B). The most upregulated protein, with a 6.1-fold upregulation, was TMEM14C (Transmembrane protein 14C), a protein located in the inner mitochondrial membrane and involved in various mitochondrial processes, including haem biosynthesis.

Gene Ontology (GO) analysis revealed that respiratory chain and mitochondrial function were the most significantly downregulated biological processes and components in PM-Mito (Fig. 4C and D).

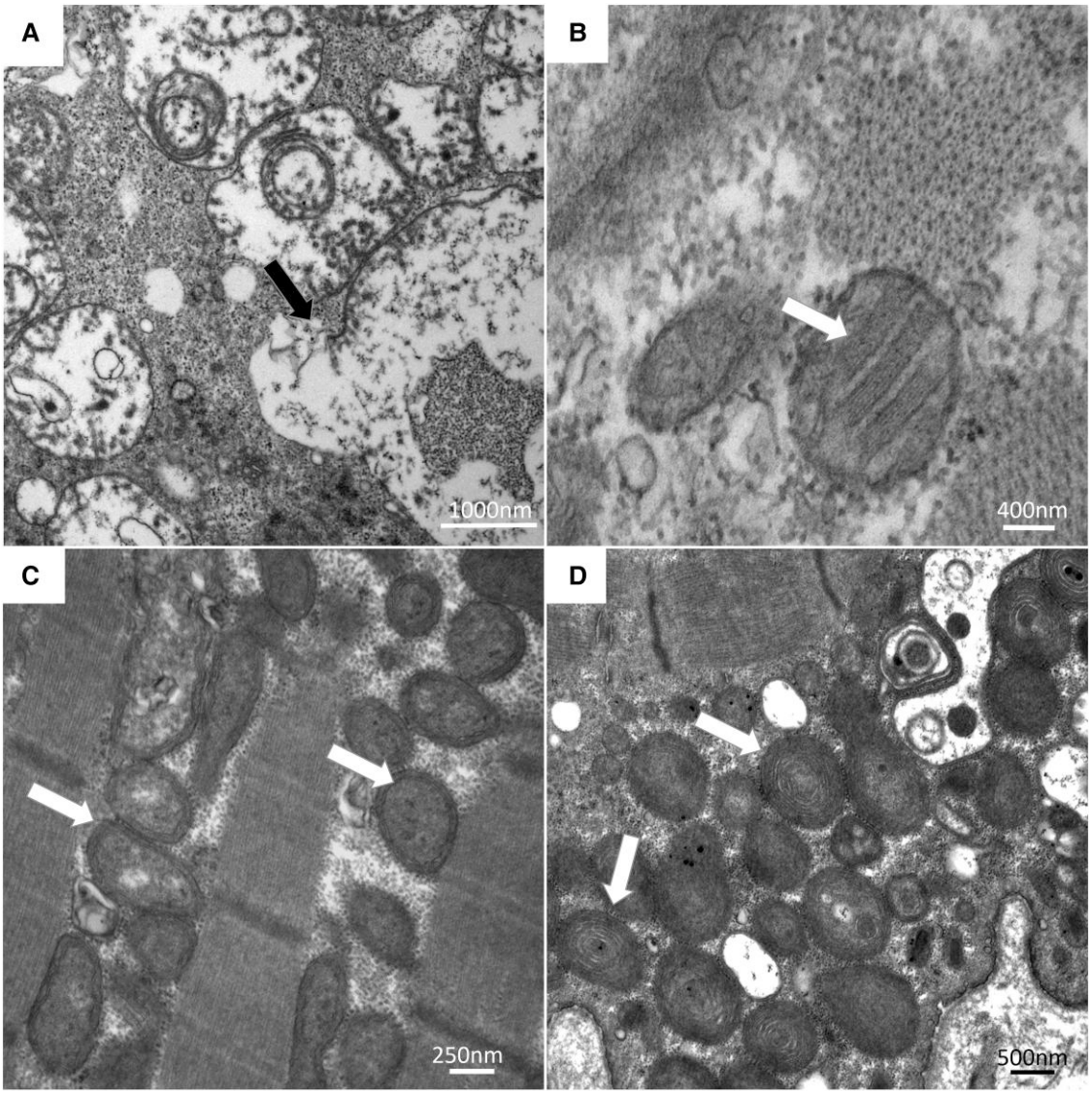

Figure 2 Ultrastructural features of abnormal mitochondria in IBM-SD. Representative images of mitochondrial pathology in PM-Mito (**A**–**C**) and IBM (**D**). (**A**) Disruption of mitochondrial membranes and leakage of mitochondrial content (arrows). (**B**) Paracrystalline inclusions (arrows). (**C**) Circular mitochondrial membranes (with lack of cristae) (arrows). (**D**) Mitochondria with densely packed concentric cristae (arrows). IBM-SD = inclusion body myositis spectrum disease; PM-Mito = polymyositis with mitochondrial pathology.

Conversely, extracellular space emerged as the most upregulated process and component in IBM skeletal muscle, possibly reflecting (fibrotic) tissue remodelling at the protein level (Fig. 4C and D).

Bulk RNA sequencing analysis of muscle biopsy specimens from nine IBM and seven PM-Mito patients revealed significant downregulation of transcripts associated with mitochondrial function. Concurrently, transcripts linked to inflammatory processes, particularly interferon-gamma signalling, were upregulated in both PM-Mito and IBM (Fig. 4E). The downregulation of mitochondrial transcripts was observed for both nuclear- and mtDNA-encoded genes, consistent with the protein-level findings (Supplementary Fig. 1 and Supplementary Tables 2 and 3).

Immunoblotting of mitochondrial membrane-associated proteins

To study the molecular underpinnings of morphological and ultrastructural abnormalities of mitochondria, we immunoblotted mitochondrial membrane-associated proteins in three PM-Mito and three IBM patient samples compared with three control samples. There was a marked decrease in key inner mitochondrial membrane proteins, including ATP5A and CHCHD3/MIC19 (Fig. 5A and B and Supplementary Figs 2 and 3). Unfortunately, in one PM-Mito sample, successful immunoblotting was achieved only for CHCHD3 and β-actin. Owing to insufficient material, it was not possible to repeat the immunoblotting on this sample.

Recent work has shown that a functional complex forms between mitochondrial proteins SAM50, ATAD3A and MIC19/MICOS (mitochondrial contact site and cristae organizing system) to maintain membrane and mtDNA stability.[31] All the proteins play key roles in the organization and maintenance of the mitochondrial membranes, including the structure of cristae. Furthermore, we saw a decrease in the mitochondrial outer membrane protein VDAC1. Given that VDAC1 is located on the outer mitochondrial membrane and is associated with mitochondrial dysfunction and mtDNA release,[32] we wanted to assess the extent of the

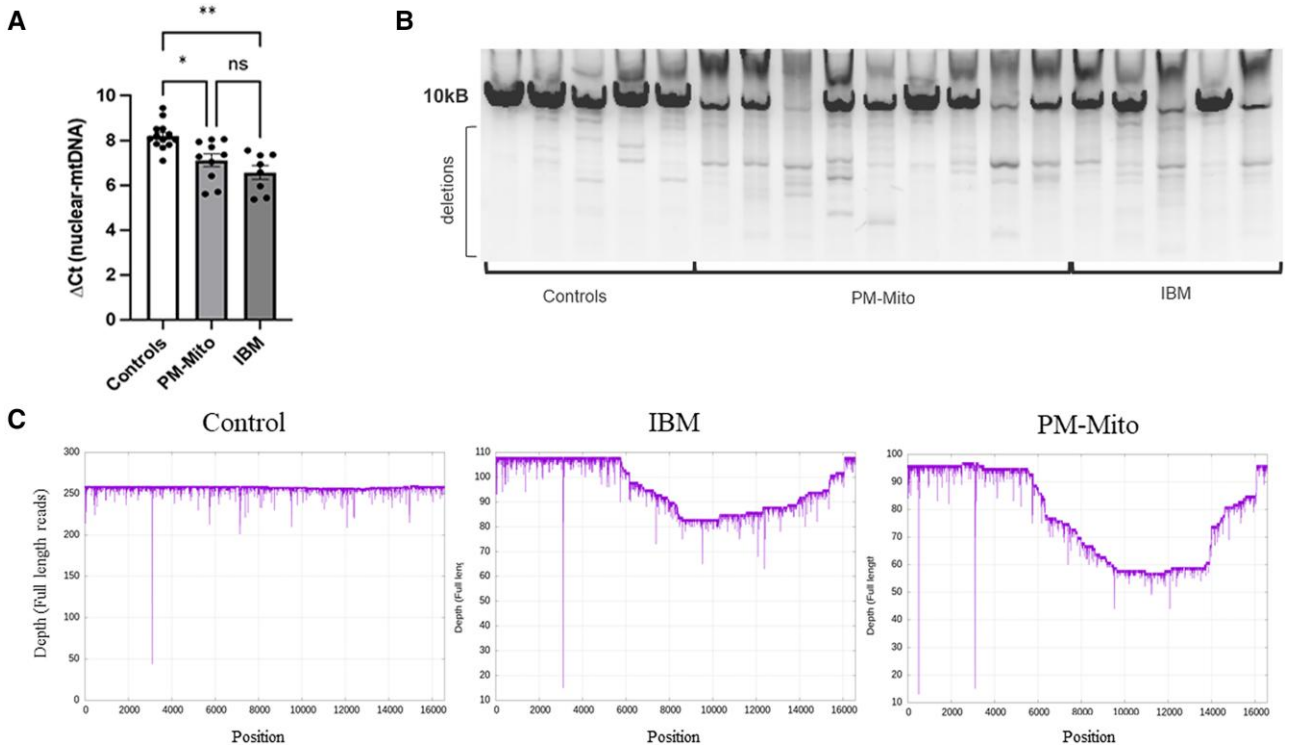

Figure 3 Alterations of mtDNA in PM-Mito and typical IBM. (**A**) Quantitative PCR based mtDNA copy number assessment showing a reduction in copy numbers in IBM-spectrum disease patients, but no significant difference between PM-Mito and IBM patients. (**B**) Long-range PCR of the mtDNA major arc showing multiple, age-inappropriate mtDNA deletions in PM-Mito ($n = 9$) and IBM ($n = 5$) muscle biopsy specimens, compared with age-matched controls ($n = 5$). (**C**) Multiplexed full-length single-molecule sequencing of mtDNA detected several medium- and large-scale deletions with similar deletion patterns in PM-Mito ($n = 8$) and IBM ($n = 9$). The multiple mtDNA deletions were detected in heteroplasmy rates between ~1% and >50%, and often covered regions from 8 to 12 kb, but deleted regions spanned 3–16 kb. The amount of mtDNA deletions was significantly higher in patients compared with age-matched controls ($n = 7$), and the heteroplasmy rate was slightly higher in PM-Mito than in late IBM. *$P = 0.0077$ and **$P = 0.0002$. IBM = inclusion body myositis; mtDNA = mitochondrial DNA; PM-Mito = polymyositis with mitochondrial pathology.

mitochondrial membrane defect in the context of PM-Mito/IBM. The results confirm the diverse spectrum of mitochondrial membrane proteins affected in this disease context.

Inflammation and mitochondrial dysfunction in PM-Mito and IBM

Activation of canonical pro-inflammatory pathways

It has previously been described that mitochondrial damage can lead to the intracellular leakage of mtDNA, which may activate the pro-inflammatory cGAS/STING pathway.[33] Therefore, after confirming the presence of widespread mitochondrial abnormalities in PM-Mito, we studied the expression levels of proteins linked to the cGAS/STING pathway by immunoblotting. We detected an upregulation of cGAS downstream targets pSTING, total STING and pro- and active forms of caspase-1 in both PM-Mito and IBM but not in control samples (Fig. 6A and C and Supplementary Fig. 4). Caspase-1 is closely linked to the cGAS/STING-mediated inflammasome assembly.[33]

Bulk RNA sequencing confirmed an upregulation of the cGAS/STING pathway in PM-Mito and typical IBM compared with controls at the gene expression level. Interestingly, cGAS/STING activation was more pronounced in PM-Mito samples at the RNA level (Supplementary Fig. 5). Further correlation analysis showed that cGAS/STING-associated transcript levels showed a positive correlation with immune cell markers (e.g. CD8, CD68) and negative correlation with markers of muscle regeneration and structure (e.g. MYH3, ACTA1; Supplementary Fig. 6).

To investigate whether the activation of DNA sensing pathways might be associated with the leakage of mtDNA, we analysed patient serum samples for cell-free mtDNA to assess its extracellular release. Cell-free mtDNA has been shown to act as a potent pro-inflammatory trigger in other diseases.[34] However, its role in activating the cGAS/STING pathway in muscle fibres has not been demonstrated conclusively.

IBM samples showed more circulating cell-free mtDNA than controls, with more than double circulating mtDNA levels of the two mitochondrial genes *MT-ND1* and *MT-ND4* (Fig. 6B). This indicated that mtDNA release from the mitochondria is prominent in IBM and might be a potential inflammatory trigger.

Inflammatory infiltrates, p62 deposits and the extent of mitochondrial pathology

To study whether the amounts of infiltrating immune cells ($CD8^+$ T cells, $CD68^+$ macrophages and $CD45^+$ leucocytes) and COX–SDH-positive cells were correlated in the PM-Mito and IBM cohorts, we performed Pearson correlation analysis. This revealed no correlation between $CD8^+$ T-cell-mediated inflammation and the extent of mitochondrial alterations (i.e. COX–SDH-positive fibres) in the PM-Mito ($P = 0.6$) and typical IBM ($P = 0.84$) cohorts. Furthermore, neither the number of $CD68^+$ macrophages (PM-Mito $P = 0.93$; typical IBM $P = 0.91$) nor the total $CD45^+$ leucocyte count (PM-Mito $P = 0.61$; typical IBM $P = 0.98$) was correlated with COX–SDH abnormalities in the patient groups. In addition, there was no correlation between the amount of $p62^+$ fibres and the extent of mitochondrial

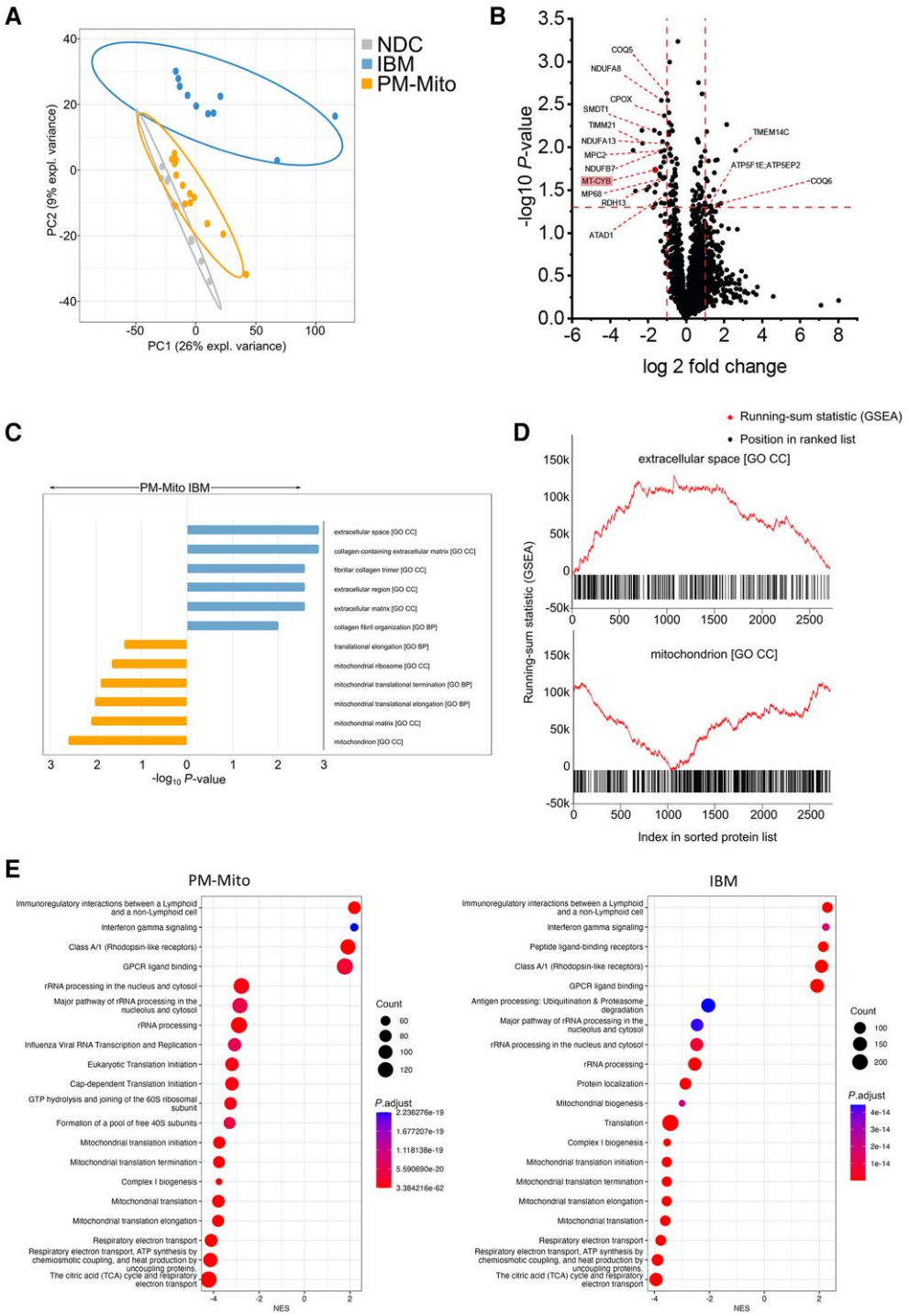

Figure 4 Unbiased proteomic profiling and bulk RNA sequencing of PM-Mito and IBM muscle biopsy specimens. (**A**–**D**) Unbiased proteomic profiling. (**E**) Bulk RNA sequencing. (**A**) Principal component analysis showing segregation of NDC, PM-Mito and IBM patients, with PM-Mito patients clustering between NDC and IBM patients. (**B**) Volcano plot illustrating dysregulated mitochondrial proteins in PM-Mito, showing a profound dysregulation of proteins associated with complexes I and III, in addition to inner mitochondrial membrane proteins. Among the dysregulated proteins, only MT-CYB (highlighted in red) represents a mitochondrial DNA-encoded protein. (**C**) Gene ontology (GO)-based gene set enrichment analysis (GSEA) for PM-Mito, including biological process (BP) ontology and cellular component (CC) ontology. Processes and components linked to extracellular remodelling and turnover are strongly enriched in IBM, whereas mitochondria-associated processes and components are negatively enriched in PM-Mito. (**D**) GSEA enrichment plots of strongly enriched cellular components from (**C**): extracellular space (IBM) and mitochondrion (PM-Mito). (**E**) GSEA dot plots illustrating RNA-sequencing data, highlighting shared dysregulated pathways in PM-Mito (*left*) and IBM (*right*). Notable findings include upregulation of inflammatory and interferon-gamma signalling pathways, alongside a pronounced downregulation of mitochondria-associated pathways. IBM = inclusion body myositis; NDC = non-disease controls; PM-Mito = polymyositis with mitochondrial pathology.

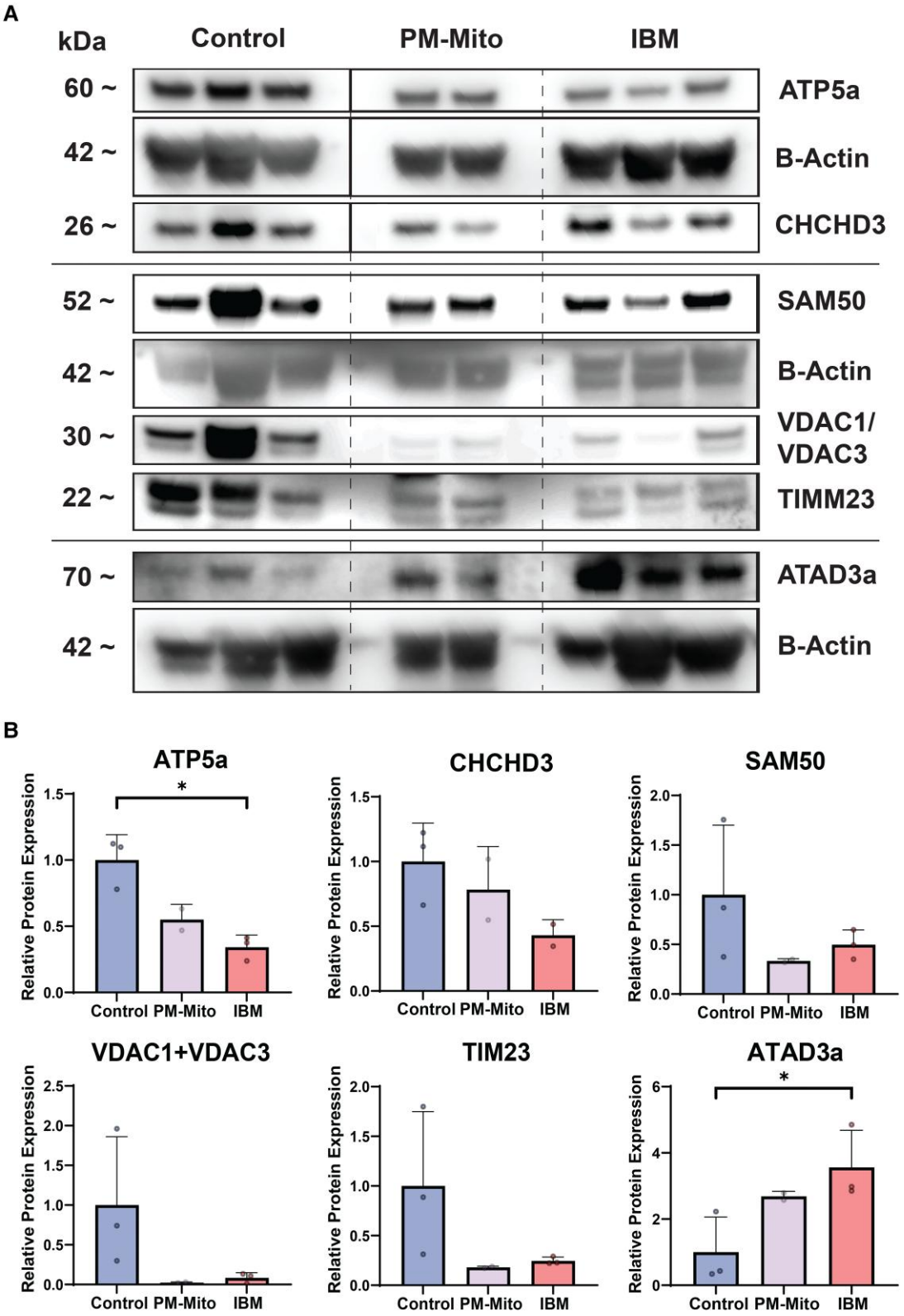

Figure 5 Structural and functional alterations of mitochondria in PM-Mito. (**A**) Representative images of immunoblotting for mitochondrial membrane proteins illustrating dysregulation of mitochondrial membrane proteins in PM-Mito ($n = 2$) compared with typical IBM ($n = 3$) and controls ($n = 3$). (**B**) Quantification of protein expression normalized to β-actin and relativized to the average of controls. *$P < 0.05$. IBM = inclusion body myositis; PM-Mito = polymyositis with mitochondrial pathology.

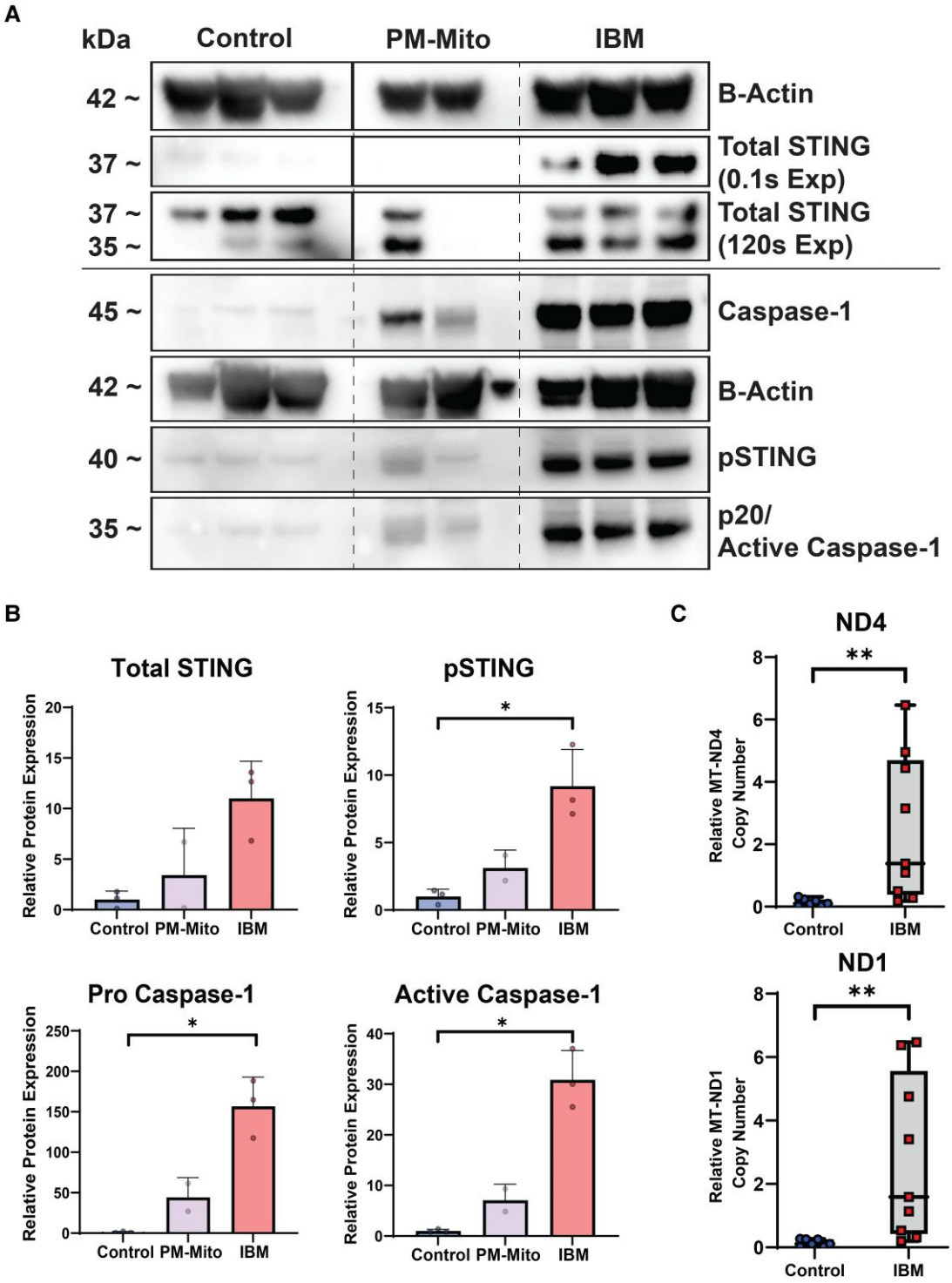

Figure 6 Mitochondria-associated inflammation in PM-Mito and typical IBM patients. (**A**) Representative images of immunoblotting for cGAS/STING-associated proteins and caspase-1. (**B**) Quantification of protein expression normalized to β-actin and relativized to the average of controls. (**C**) Cell-free mtDNA quantification of mitochondrial genes *MT-ND1* and *MT-ND4* from the serum of IBM patients showed elevated levels of circulating mtDNA in the patient group ($n = 9$) compared with controls ($n = 7$), indicating a leakage of mtDNA from muscle cells into the blood. $^{*}P < 0.05$ and $^{**}P < 0.01$. cGAS/STING = cyclic GMP–AMP synthase/stimulator of interferon genes; IBM = inclusion body myositis; mtDNA = mitochondrial DNA; PM-Mito = polymyositis with mitochondrial pathology.

alterations (i.e. COX–SDH-positive fibres; $P = 0.56$) and $CD8^{+}$ infiltrates ($P = 0.45$) in the IBM cohort. There was no spatial association between COX–SDH abnormalities and the distribution of inflammatory infiltrates.

Discussion

This study focused on mitochondrial alterations as an early feature of IBM pathophysiology. To study this, we investigated PM-Mito as

an early form of IBM. We observed mitochondrial abnormalities in both PM-Mito and typical IBM at the histological, ultrastructural and molecular levels. The numbers of COX-negative fibres were similar and higher than expected according to the age of the patients in both PM-Mito and IBM. The extent of mitochondrial damage was not correlated with the amount of inflammation, suggesting no causative effect. Abnormalities such as disorganized and circular mitochondrial membranes, along with enlarged and dysmorphic mitochondria, were prevalent in both PM-Mito and IBM patients. Interestingly, ultrastructural abnormalities also included disturbed cristae architecture and discontinuity of the mitochondrial membranes, allowing leakage of mitochondrial content into the sarcoplasm.

Furthermore, elevated levels of cell-free mtDNA were detected in the blood samples of IBM patients. Multiple large-scale mtDNA deletions and reduced copy numbers were evident in PM-Mito compared with healthy age-matched controls. Notably, there was no significant difference in these mitochondrial DNA alterations between the PM-Mito and IBM groups. Additionally, structural proteins of the inner mitochondrial membrane also involved in quality control of the membrane and mtDNA (SAM50, ATAD3A and MIC19/MICOS) were differentially regulated in PM-Mito and IBM samples compared with age-matched control muscle. Immunoblotting confirmed dysregulation of proteins related to mitochondrial ultrastructure and MICOS (e.g. TIM21, SMDT1), thus validating data on unbiased proteomic and transcriptomic profiling. We observed activation of the canonical cGAS/STING pathway at various stages of IBM-SD (in both PM-Mito and IBM), indicating that the release of mitochondrial DNA from cells, along with subsequent activation of the innate immune response, might play a role in the underlying mechanisms involved. PM-Mito and IBM share significant similarities in mitochondrial abnormalities, including the presence of COX-negative fibres, ultrastructural defects and large-scale mtDNA deletions, demonstrating that mitochondrial dysfunction is a central and early feature in both conditions. Although PM-Mito is likely to represent an early form of IBM, there are subtle differences, such as the presence of giant mitochondria with pronounced ultrastructural abnormalities observed predominantly in late-stage IBM. This finding is likely to result from advanced disease progression and does not indicate fundamental differences in pathophysiology. Importantly, we demonstrate that mitochondrial dysfunction occurs before the onset of fibrotic tissue remodelling and cellular inflammatory infiltrates, reinforcing that it is an upstream event in the disease cascade.

Furthermore, mitochondrial abnormalities are not correlated with the degree of inflammation, suggesting that they are not secondary effects of inflammation but are integral to disease pathogenesis. These findings corroborate our earlier work,[27] which had shown that mitochondrial dysfunction is a key aspect of IBM-SD, highlighting its importance as a main factor rather than only a result of ongoing inflammation. However, the specific causes of these mitochondrial issues still need to be clarified. A potential limitation in this context is the impact of the biopsy site on vacuole detection, which might have resulted in some IBM patients being diagnosed as PM-Mito. Given that IBM is likely to be a progressive disease with various stages, such variability is inherent to its pathogenesis.

In general, mitochondrial abnormalities are not a typical feature of idiopathic inflammatory myopathies, with the exception of dermatomyositis showing perifascicular COX-SDH abnormalities.[35,36] However, the molecular mechanisms underlying mitochondrial dysfunction in dermatomyositis differ from those observed in IBM, because single point mutations and depletion of the mtDNA in dermatomyositis[37] have been restricted to focal areas with inflammatory infiltrates.[38] In contrast, IBM muscle is characterized by large-scale deletions in the major arc of mtDNA molecules[39] and lower mtDNA copy numbers than healthy subjects of similar age groups.[40]

We could reproduce these findings in both cohorts of PM-Mito and IBM patients, further substantiating the involvement of mitochondrial dysfunction in these conditions.

At the protein level, combined unbiased proteomic analysis and immunoblotting highlight the involvement of the inner mitochondrial membrane, as evidenced by the downregulation of TIM21 and TIM23, which are close interaction partners within the inner mitochondrial membrane protein complex.[41] The disruption of this intricate protein network is likely to contribute to altered mitochondrial ultrastructure, impaired mtDNA replication and, possibly, release of mtDNA. Consistent with these molecular findings, previous studies have demonstrated significant morphological abnormalities in IBM myofibres, including shortened and enlarged cristae, membrane disruption and a reduced mitochondrial length-to-width ratio.[42] We observed giant mitochondria with highly abnormal cristae, which were almost exclusively detected in IBM, but not in PM-Mito, suggesting that these ultrastructural abnormalities develop at a later stage. This peculiar ultrastructural abnormality has already been described in the context of IBM.[29,43] Our ultrastructural data clearly showed similar patterns in PM-Mito and IBM, underlining the functional impact of the dysregulation of (inner) mitochondrial membrane proteins. However, it is also important to acknowledge that the mitochondrial ultrastructural abnormalities reported here are not specific to IBM-SD. Similar changes have been described in other conditions characterized by profound mitochondrial dysfunction, including mitochondrial myopathies. As an example, skeletal muscle biopsies of patients with m.8344A>G mutations show similar ultrastructural abnormalities.[44]

Another relevant ultrastructural feature observed in this study was the disruption of mitochondrial membranes and leakage of mitochondrial content into the sarcoplasm. The release of mtDNA and mitochondrial content into the cytosol has been described to act as mitochondrial-derived damage-associated molecular pattern (DAMP),[34] triggering inflammatory cascades such as the cGAS/STING pathway.[33,45] DAMPs are recognized as foreign by the pattern recognition receptors of the immune system, and this triggers the activation of pro-inflammatory pathways, such as toll-like receptor (TLR) signalling.[46] For example, the binding of oxidized cardiolipins to TLR4 in the cytosol can initiate nuclear factor-κB signalling, leading to increased myostatin expression, which has been detected in IBM muscle.[47] Thus, it is possible that the profound mitochondrial abnormalities observed in PM-Mito could trigger canonical inflammatory pathways, further contributing to the disease progression. Testing this hypothesis, we observed an upregulation of the cGAS/STING pathway at both RNA and protein levels in our PM-Mito and IBM cohorts. This finding is particularly relevant, because it indicates a significant role of mitochondria-associated inflammation in the early pathophysiology of IBM-SD, i.e. before fatty–fibrotic tissue remodelling and massive lymphocytic infiltration are observed. Interestingly, it has been shown that IBM is characterized by a distinct interferon signature at the gene expression level, with a predominance of type II interferons.[48] This interferon signature was also clearly evident in our transcriptomic data. The downstream effects of STING, a potent transcriptional activator of interferon-stimulated genes, might explain this signature.[49]

Interestingly, a recent study demonstrated that increased circulating cell-free mtDNA levels are associated with the activation of

the cGAS/STING pathway in primary mitochondrial diseases (mitochondrial encephalomyopathy, lactic acidosis, and stroke-like episodes and chronic progressive external ophthalmoplegia).[50] This finding provides additional support to our hypothesis that mitochondrial dysfunction, including mtDNA release, contributes to the activation of inflammatory pathways in IBM, further highlighting the relevance of mitochondrial-derived DAMPs in the early stages of the disease. However, the evidence for mtDNA release into the cytosol in this study is indirect, based on ultrastructural observations and the presence of circulating cell-free mtDNA. To gain a better understanding of mtDNA release in the context of PM-Mito and IBM, appropriate techniques (e.g. for *in situ* visualization within muscle cells) are needed. Future studies will be essential to address significant methodological challenges and provide direct evidence for mtDNA release in muscle tissue.

On the morphological level, the prominent upregulation of MHC class I in PM-Mito also clearly indicates a role for interferon type I in the pathogenesis of the disease. In this context, the release of IFN-II (i.e. IFN-gamma), which has been well described in IBM, might be explained by downstream effects of IFN-I and persistence of a pro-inflammatory milieu, leading to the invasion of IFN-gamma-releasing immune cells (e.g. $CD4^+$ T cells, macrophages). However, this interplay warrants further investigation. Our data indicate that these immune phenomena might be secondary to mitochondrial dysfunction and associated inflammation in the IBM cascade. This, in turn, could suggest that IBM can be viewed as a primarily degenerative disease with peculiar (auto-)inflammatory features. Indeed, recently published data from mouse xenograft models pointed towards IBM being a primarily degenerative disease of skeletal muscle,[51] in which inflammation might be a bystander or a secondary phenomenon. Although supported by the early and extensive mitochondrial dysfunction observed in our study, this hypothesis remains unproved and warrants further investigation to clarify the temporal and mechanistic relationship between degenerative processes and inflammatory features in IBM-SD.

We detected large-scale deletions of mtDNA in PM-Mito patients, raising the possibility that mtDNA damage could be a primary cause of mitochondrial dysfunction in IBM-SD. Long-range PCR allowed for the detection of higher heteroplasmy rates of mtDNA deletions in IBM and PM-Mito samples, and single-molecule long-read sequencing provided a more sensitive and precise mapping of these deletions, highlighting the methodological differences between these approaches. Several explanations for these mtDNA deletions in the context of IBM have been discussed: errors in DNA replication, accumulation of reactive oxygen species, impaired DNA repair systems, and defective autophagy (mitophagy).[52] Moreover, the reduced mtDNA copy numbers point towards an mtDNA maintenance defect. Notably, single nucleotide polymorphisms in key genes involved in mtDNA replication and maintenance, such as the DNA helicase Twinkle, DNA polymerase γ (*POLG*) and ribonucleotide-diphosphate reductase subunit M2B (*RRM2B*), have been identified in IBM patients.[53] However, no significant differences in variant prevalence in *POLG* were found between the IBM groups or between IBM patients and the control population. Thus, the pathogenic role of these single nucleotide polymorphisms has not been demonstrated convincingly.[53] We hypothesize that the multiple mtDNA deletions and depletion might be related to the severe abnormalities of mitochondrial cristae, where mtDNA replication occurs. Whether variants in nuclear genes involved in mtDNA replication have a modifying role on this process is currently unclear. However, understanding the exact mechanism of these events requires further studies.

Another interesting hypothesis, derived from studies performed in the context of amyotrophic lateral sclerosis, links mitochondrial damage and the release of mtDNA to the deposition of TDP-43 in the cytosol and in mitochondria.[54] Indeed, TDP-43 mislocalization and sarcoplasmic deposition are characteristic, but not specific, features observed in IBM muscle.[55] We and others recently demonstrated the presence of TDP-43-associated cryptic exons in IBM muscle,[2,51] pointing towards a potential functional impact of TDP-43 pathology.

Lastly, from a clinical perspective, patients with PM-Mito present a spectrum of clinical symptoms, including non-specific complaints, such as myalgia. Defining the onset of the disease in this cohort is challenging, because IBM-SD might begin insidiously, with vague, non-specific symptoms. Therefore, previous and present studies might have missed even earlier forms of the disease, and the progression of this diverse phenotype into the characteristic clinical pattern of IBM remains unclear. Recently published studies on muscle MRI patterns in PM-Mito have yielded conflicting results, showing muscle involvement patterns similar to IBM in one[56] and partly different patterns in another study.[57] However, the data reported here again illustrate the considerable molecular overlap between PM-Mito and IBM, underlining the importance of considering IBM as a disease spectrum with early and late stages.

Conclusion

In conclusion, this study established mitochondrial abnormalities as an early and characteristic finding in IBM-SD. PM-Mito and typical IBM did not differ significantly regarding mitochondrial morphology, ultrastructure and molecular characteristics of mitochondrial damage. Based on our data, we hypothesize that inflammation might not induce mitochondrial dysfunction in a time-dependent manner; instead, mitochondrial dysfunction appears to be an early event in disease pathogenesis. Considering ongoing IBM clinical trials with immunosuppressants, this finding might have important implications for clinical practice.

Data availability

The data supporting the findings of this study are available from the corresponding authors, R.H. and W.S., upon reasonable request. The mass spectrometry proteomics data have been deposited to the ProteomeXchange Consortium via the PRIDE partner repository,[22] with the dataset identifier PXD053742.

Funding

We thank the Deutsche Gesellschaft für Muskelkranke (DGM) e.V. for funding this study. A.H. acknowledges the support by the Ministerium für Kultur und Wissenschaft des Landes Nordrhein-Westfalen, the Regierenden Bürgermeister von Berlin-Senatskanzlei Wissenschaft und Forschung and the Bundesministerium für Bildung und Forschung. The European Regional Development Fund (ERDF) financed parts of this study in the framework of the NME-GPS project (grant to A.R.). R.H. is supported by the Wellcome Trust (Wellcome Discovery Award 226653/Z/22/Z), the Medical Research Council (United Kingdom) (MR/V009346/1), the Addenbrookes Charitable Trust Cambridge University Hospitals (G100142), the Evelyn Trust, the Stoneygate Trust, the Lily Foundation, Ataxia UK, Action for AT, Muscular Dystrophy UK London, LifeArc (LAC-TreatMito) and the UKRI/

Horizon Europe Guarantee MSCA Doctoral Network Programme (Project 101120256: MMM). She is also supported by an MRC strategic award to establish an International Centre for Genomic Medicine in Neuromuscular Diseases (ICGNMD) MR/S005021/1 and by the NIHR Cambridge Biomedical Research Centre (BRC-1215-20014). The views expressed are those of the authors and not necessarily those of the NIHR or the Department of Health and Social Care. CNAG: This project received funding from the European Commission (Horizon 2020 programme, grant agreement No. 824110).

Competing interests

K.H. received financial reimbursement for consulting, advisory board activities, speaker fees and/or contributions to congresses and travel support to attend scientific meetings by Akcea Therapeuticals Inc., Alnylam Pharmaceuticals Inc., Amicus, AstraZeneca, GSK, Hormosan, Takeda Pharmaceutical Inc., Pfizer Pharmaceuticals Inc., Swedish Orphan Biovitrum Inc. and ViiV Healthcare GmbH. K.H. also received research funding by the foundation Charité (BIH clinical fellow), Alnylam Pharmaceuticals Inc. and Pfizer Pharmaceuticals. None of this is related to the present work.

Supplementary material

Supplementary material is available at *Brain* online.

References

1. Blume G, Pestronk A, Frank B, Johns DR. Polymyositis with cytochrome oxidase negative muscle fibres. Early quadriceps weakness and poor response to immunosuppressive therapy. *Brain*. 1997;120(Pt 1):39-45.
2. Kleefeld F, Uruha A, Schänzer A, et al. Morphological and molecular patterns of polymyositis with mitochondrial pathology and inclusion body myositis. *Neurology*. 2022;99:e2212-e2222.
3. Santorelli FM, Sciacco M, Tanji K, et al. Multiple mitochondrial DNA deletions in sporadic inclusion body myositis: A study of 56 patients. *Ann Neurol*. 1996;39:789-795.
4. Horvath R, Fu K, Johns T, Genge A, Karpati G, Shoubridge EA. Characterization of the mitochondrial DNA abnormalities in the skeletal muscle of patients with inclusion body myositis. *J Neuropathol Exp Neurol*. 1998;57:396-403.
5. Hedberg-Oldfors C, Lindgren U, Basu S, et al. Mitochondrial DNA variants in inclusion body myositis characterized by deep sequencing. *Brain Pathol*. 2021;31:e12931.
6. Zhou M, Cheng X, Zhu W, et al. Activation of cGAS-STING pathway—A possible cause of myofiber atrophy/necrosis in dermatomyositis and immune-mediated necrotizing myopathy. *J Clin Lab Anal*. 2022;36:e24631.
7. Wilkinson MGL, Moulding D, McDonnell TCR, et al. Role of CD14 + monocyte-derived oxidised mitochondrial DNA in the inflammatory interferon type 1 signature in juvenile dermatomyositis. *Ann Rheum Dis*. 2023;82:658-669.
8. Skopelja-Gardner S, An J, Elkon KB. Role of the cGAS-STING pathway in systemic and organ-specific diseases. *Nat Rev Nephrol*. 2022;18:558-572.
9. Huntley ML, Gao J, Termsarasab P, et al. Association between TDP-43 and mitochondria in inclusion body myositis. *Lab Invest*. 2019;99:1041-1048.
10. Askanas V, Engel WK. Sporadic inclusion-body myositis: Conformational multifactorial ageing-related degenerative muscle disease associated with proteasomal and lysosomal inhibition, endoplasmic reticulum stress, and accumulation of amyloid-β42 oligomers and phosphorylated tau. *La Presse Médicale*. 2011;40(Pt 2):e219-e235.
11. Callender LA, Carroll EC, Beal RWJ, et al. Human $CD8^+$ EMRA T cells display a senescence-associated secretory phenotype regulated by p38 MAPK. *Aging Cell*. 2018;17:e12675.
12. Benveniste O, Allenbach Y. Inclusion body myositis: Accumulation of evidence for its autoimmune origin. *Brain*. 2019;142:2549-2551.
13. Rigolet M, Hou C, Baba Amer Y, et al. Distinct interferon signatures stratify inflammatory and dysimmune myopathies. *RMD Open*. 2019;5:e000811.
14. Yamashita S, Tawara N, Zhang Z, et al. Pathogenic role of anti-cN1A autoantibodies in sporadic inclusion body myositis. *J Neurol Neurosurg Psychiatry*. 2023;94:1018-1024.
15. Lilleker JB, Naddaf E, Saris CGJ, et al. 272nd ENMC international workshop: 10 years of progress—Revision of the ENMC 2013 diagnostic criteria for inclusion body myositis and clinical trial readiness. 16–18 June 2023, Hoofddorp, The Netherlands. *Neuromuscul Disord*. 2024;37:36-51.
16. Preuße C, Goebel HH, Held J, et al. Immune-mediated necrotizing myopathy is characterized by a specific Th1-M1 polarized immune profile. *Am J Pathol*. 2012;181:2161-2171.
17. Preuße C, Allenbach Y, Hoffmann O, et al. Differential roles of hypoxia and innate immunity in juvenile and adult dermatomyositis. *Acta Neuropathol Commun*. 2016;4:45.
18. Udd B, Stenzel W, Oldfors A, et al. 1st ENMC European meeting: The EURO-NMD pathology working group Recommended Standards for Muscle Pathology Amsterdam, The Netherlands, 7 December 2018. *Neuromuscul Disord*. 2019;29:483-485.
19. Kleefeld F, Horvath R, Pinal-Fernandez I, et al. Multi-level profiling unravels mitochondrial dysfunction in myotonic dystrophy type 2. *Acta Neuropathol*. 2024;147:19.
20. Gangfuß A, Hentschel A, Heil L, et al. Proteomic and morphological insights and clinical presentation of two young patients with novel mutations of *BVES (POPDC1)*. *Mol Genet Metab*. 2022;136:226-237.
21. Ladislau L, Suárez-Calvet X, Toquet S, et al. JAK inhibitor improves type I interferon induced damage: Proof of concept in dermatomyositis. *Brain*. 2018;141:1609-1621.
22. Perez-Riverol Y, Bai J, Bandla C, et al. The PRIDE database resources in 2022: A hub for mass spectrometry-based proteomics evidences. *Nucleic Acids Res*. 2022;50:D543-D552.
23. Hathazi D, Griffin H, Jennings MJ, et al. Metabolic shift underlies recovery in reversible infantile respiratory chain deficiency. *EMBO J*. 2020;39:e105364.
24. Keraite I, Becker P, Canevazzi D, et al. A method for multiplexed full-length single-molecule sequencing of the human mitochondrial genome. *Nat Commun*. 2022;13:5902.
25. Pinal-Fernandez I, Casal-Dominguez M, Derfoul A, et al. Machine learning algorithms reveal unique gene expression profiles in muscle biopsies from patients with different types of myositis. *Ann Rheum Dis*. 2020;79:1234-1242.
26. Subramanian A, Tamayo P, Mootha VK, et al. Gene set enrichment analysis: A knowledge-based approach for interpreting genome-wide expression profiles. *Proc Natl Acad Sci U S A*. 2005;102:15545-15550.
27. Kleefeld F, Uruha A, Schänzer A, et al. Morphologic and molecular patterns of polymyositis with mitochondrial pathology and inclusion body myositis. *Neurology*. 2022;99:e2212-e2222.
28. Fayet G, Jansson M, Sternberg D, et al. Ageing muscle: Clonal expansions of mitochondrial DNA point mutations and deletions cause focal impairment of mitochondrial function. *Neuromuscul Disord*. 2002;12:484-493.

29. Carpenter S. Inclusion body myositis, a review. *J Neuropathol Exp Neurol*. 1996;55:1105-1114.
30. Chen T, He J, Huang Y, Zhao W. The generation of mitochondrial DNA large-scale deletions in human cells. *J Hum Genet*. 2011;56:689-694.
31. Dong J, Chen L, Ye F, et al. Mic19 depletion impairs endoplasmic reticulum-mitochondrial contacts and mitochondrial lipid metabolism and triggers liver disease. *Nat Commun*. 2024;15:168.
32. Kim J, Gupta R, Blanco LP, et al. VDAC oligomers form mitochondrial pores to release mtDNA fragments and promote lupus-like disease. *Science (New York, NY)*. 2019;366:1531-1536.
33. Kim J, Kim H-S, Chung JH. Molecular mechanisms of mitochondrial DNA release and activation of the cGAS-STING pathway. *Exp Mol Med*. 2023;55:510-519.
34. Tumburu L, Ghosh-Choudhary S, Seifuddin FT, et al. Circulating mitochondrial DNA is a proinflammatory DAMP in sickle cell disease. *Blood*. 2021;137:3116-3126.
35. Alhatou MI, Sladky JT, Bagasra O, Glass JD. Mitochondrial abnormalities in dermatomyositis: Characteristic pattern of neuropathology. *J Mol Histol*. 2004;35:615-619.
36. Schänzer A, Rager L, Dahlhaus I, et al. Morphological characteristics of idiopathic inflammatory myopathies in juvenile patients. *Cells*. 2022;11:109.
37. Hedberg-Oldfors C, Lindgren U, Visuttijai K, et al. Respiratory chain dysfunction in perifascicular muscle fibres in patients with dermatomyositis is associated with mitochondrial DNA depletion. *Neuropathol Appl Neurobiol*. 2022;48:e12841.
38. Meyer A, Laverny G, Allenbach Y, et al. IFN-β-induced reactive oxygen species and mitochondrial damage contribute to muscle impairment and inflammation maintenance in dermatomyositis. *Acta Neuropathol*. 2017;134:655-666.
39. Oldfors A, Moslemi AR, Jonasson L, Ohlsson M, Kollberg G, Lindberg C. Mitochondrial abnormalities in inclusion-body myositis. *Neurology*. 2006;66(Suppl 1):S49-S55.
40. Bhatt PS, Tzoulis C, Balafkan N, et al. Mitochondrial DNA depletion in sporadic inclusion body myositis. *Neuromuscul Disord*. 2019;29:242-246.
41. Mick DU, Dennerlein S, Wiese H, et al. MITRAC links mitochondrial protein translocation to respiratory-chain assembly and translational regulation. *Cell*. 2012;151:1528-1541.
42. Oikawa Y, Izumi R, Koide M, et al. Mitochondrial dysfunction underlying sporadic inclusion body myositis is ameliorated by the mitochondrial homing drug MA-5. *PLoS One*. 2020;15:e0231064.
43. Askanas V, Engel WK, Nogalska A. Sporadic inclusion-body myositis: A degenerative muscle disease associated with aging, impaired muscle protein homeostasis and abnormal mitophagy. *Biochim Biophys Acta*. 2015;1852:633-643.
44. Vincent AE, Ng YS, White K, et al. The spectrum of mitochondrial ultrastructural defects in mitochondrial myopathy. *Sci Rep*. 2016;6:30610.
45. Marchi S, Guilbaud E, Tait SWG, Yamazaki T, Galluzzi L. Mitochondrial control of inflammation. *Nat Rev Immunol*. 2023;23:159-173.
46. Picca A, Faitg J, Auwerx J, Ferrucci L, D'Amico D. Mitophagy in human health, ageing and disease. *Nat Metab*. 2023;5:2047-2061.
47. Sachdev R, Kappes-Horn K, Paulsen L, et al. Endoplasmic reticulum stress induces myostatin high molecular weight aggregates and impairs mature myostatin secretion. *Mol Neurobiol*. 2018;55:8355-8373.
48. Pinal-Fernandez I, Casal-Dominguez M, Derfoul A, et al. Identification of distinctive interferon gene signatures in different types of myositis. *Neurology*. 2019;93:e1193-e1204.
49. Decout A, Katz JD, Venkatraman S, Ablasser A. The cGAS–STING pathway as a therapeutic target in inflammatory diseases. *Nat Rev Immunol*. 2021;21:548-569.
50. Zhao X, Yu M, Zhao Y, et al. Circulating cell-free mtDNA release is associated with the activation of cGAS-STING pathway and inflammation in mitochondrial diseases. *J Neurol*. 2022;269:4985-4996.
51. Britson KA, Ling JP, Braunstein KE, et al. Loss of TDP-43 function and rimmed vacuoles persist after T cell depletion in a xenograft model of sporadic inclusion body myositis. *Sci Transl Med*. 2022;14:eabi9196.
52. Rygiel KA, Miller J, Grady JP, Rocha MC, Taylor RW, TurnbullDM. Mitochondrial and inflammatory changes in sporadic inclusion body myositis. *Neuropathol Appl Neurobiol*. 2015;41:288-303.
53. Lindgren U, Roos S, Oldfors CH, Moslemi A-R, Lindberg C, Oldfors A. Mitochondrial pathology in inclusion body myositis. *Neuromuscul Disord*. 2015;25:281-288.
54. Yu CH, Davidson S, Harapas CR, et al. TDP-43 triggers mitochondrial DNA release via mPTP to activate cGAS/STING in ALS. *Cell*. 2020;183:636-649.e18.
55. Olivé M, Janué A, Moreno D, Gámez J, Torrejón-Escribano B, Ferrer I. TAR DNA-binding protein 43 accumulation in protein aggregate myopathies. *J Neuropathol Exp Neurol*. 2009;68:262-273.
56. Cavalcante WCP, da Silva AMS, Mendonça RH, et al. Whole-body muscle magnetic resonance imaging in inflammatory myopathy with mitochondrial pathology. *Front Neurol*. 2024;15:1386293.
57. Zierer L-K, Naegel S, Schneider I, et al. Quantitative whole-body muscle MRI in idiopathic inflammatory myopathies including polymyositis with mitochondrial pathology: Indications for a disease spectrum. *J Neurol*. 2024;271:3186-3202.